Polarized vertical beaming of an engineered hexapole mode laser

Ju-Hyung Kang[1,*], Min-Kyo Seo[1], Sun-Kyung Kim[2], Se-Heon Kim[1], Myung-Ki Kim[1], Hong-Gyu Park[3], Ki-Soo Kim[4], and Yong-Hee Lee[1,5]

[1]Department of Physics, Korea Advanced Institute of Science and Technology, Daejeon 305-701, Korea
[2]Advanced Technology Lab, LED Division, LG Innotek, Seoul 137-724, Korea
[3]Department of Physics, Korea University, Seoul 136-701, Korea
[4]Convergence and Components & Materials Research Laboratory, Electronics and Telecommunications Research Institute, Daejeon 305-700, Korea
[5]Department of Physics and Department of Nanoscience and Technology (WCU), Korea Advanced Institute of Science and Technology, Daejeon 305-701, Korea
[*]Corresponding author: kangjuhy@kaist.ac.kr

Abstract: We demonstrate vertical beaming of linearly-polarized light from the hexapole mode of an engineered single-cell photonic crystal cavity by employing the solid angle scanning system. The vertical emission that is forbidden by the inner symmetry of the hexapole mode is made possible by perturbing its symmetry. Experimentally 56% of photons are funneled within a divergence angle of ±30°. Measured polarization-resolved far-field profiles of the engineered hexapole mode agree well with those of the predictions of finite difference time domain methods.

OCIS codes: (230.5298) Photonic crystals; (220.4241) Nanostructure fabrication; (140.3945) Microcavities; (350.4238) Nanophotonics and photonic crystals

References and links

1. O. Painter, R. Lee, A. Scherer, A. Yariv, J. O'Brien, P. Dapkus, and I. Kim, "Two-Dimensional Photonic Band-Gap Defect Mode Laser," Science **284**, 1819-1821 (1999).
2. H. -Y. Ryu, S. -H. Kim, H. -G. Park, J. -K. Hwang, Y. -H. Lee, and J. -S. Kim, "Square-lattice photonic band-gap single-cell laser operating in the lowest-order whispering gallery mode," Appl. Phys. Lett. **80**, 3883-3885 (2002).
3. T. Baba, D. Sano, K. Nozaki, K. Inoshita, Y. Kuroki, and F. Koyama, "Observation of fast spontaneous emission decay in GaInAsP photonic crystal point defect nanocavity at room temperature," Appl. Phys. Lett. **85**, 3989-3991 (2004).
4. H.-Y. Ryu, M. Notomi, and Y.-H. Lee, "High-quality-factor and small-mode-volume hexapole modes in photonic-crystal-slab nanocavities," Appl. Phys. Lett. **83**, 4294-4296 (2003).
5. K. Nozaki, S. Kita, and T. Baba, "Room temperature continuous wave operation and controlled spontaneous emission in ultrasmall photonic crystal nanolaser," Opt. Express **15**, 7506-7514 (2007).
6. A. Badolato, K. Hennessy, M. Atature, J. Dreiser, E. Hu, P. M. Petroff, and A. Imamoglu, "Deterministic coupling of single quantum dots to single nanocavity modes," Science **308**, 1158-1161 (2005).
7. D. Englund, D. Fattal, E. Waks, G. Solomon, B. Zhang, T. Nakaoka, Y. Arakawa, Y. Yamamoto, and J. Vŭcković, "Controlling the spontaneous emission rate of single quantum dots in a two-dimensional photonic crystal," Phys. Rev. Lett. **95**, 013904 (2005).
8. H. Altug, D. Englund, and J. Vŭcković, "Ultra-fast photonic crystal nanolasers," Nat. Phys. **2**, 484-488 (2006).
9. M. Lončar, A. Scherer, and Y. Qiu, "Photonic crystal laser sources for chemical detection," Appl. Phys. Lett. **82**, 648-650 (2003).
10. S.-H. Kim, J.-H. Choi, S.-K. Lee, S.-H. Kim, S.-M. Yang, Y.-H. Lee, C. Seassal, P. Regrency, and P. Viktorovitch, "Optofluidic integration of a photonic crystal nanolaser," Opt. Express **16**, 6515-6527 (2008).
11. S. Kita, K. Nozaki, and T. Baba, "Refractive index sensing utilizing a cw photonic crystal nanolaser and its array configuration," Opt. Express **16**, 8174-8180 (2008).
12. K. Srinivasan and O. Painter, "Momentum space design of high-Q photonic crystal optical cavities," Opt. Express **10**, 670-684 (2002).
13. O. Painter and K. Srinivasan, "Polarization properties of dipolelike defect modes in photonic crystal nanocavities," Opt. Lett. **27**, 339-341 (2002).

#107732 - $15.00 USD Received 24 Feb 2009; revised 28 Mar 2009; accepted 28 Mar 2009; published 31 Mar 2009

14. C. Grillet, C. Monat, C. L. Smith, B. J. Eggleton, D. J. Moss, S. Frédérick, D. Dalacu, P. J. Poole, J. Lapointe, G. Aers, and R. L. Williams, "Nanowire coupling to photonic crystal nanocavities for single photon sources," Opt. Express **15**, 1267-1276 (2007).
15. H.-G. Park, S.-H. Kim, S.-H. Kwon, Y.-G. Ju, J.-K. Yang, J.-H. Baek, S.-B. Kim, and Y.-H. Lee, "Electrically driven single-cell photonic crystal laser," Science **305**, 1444-1447 (2004).
16. M. -K. Seo, K. -Y. Jeong, J.-K. Yang, Y.-H. Lee, H.-G. Park, and S.-B. Kim, "Low threshold current single-cell hexapole mode photonic crystal laser," Appl. Phys. Lett. **90**, 171122 (2007).
17. H.-G. Park, J.-K. Hwang, J. Huh, H.-Y. Ryu, S.-H. Kim, J.-S. Kim, and Y.-H. Lee, "Characteristics of modified single-defect two-dimensional photonic crystal lasers," IEEE J. Quantum Electron. **38**, 1353-1365 (2002).
18. S.-H. Kim, S.-K. Kim, and Y.-H. Lee, "Vertical beaming of wavelength-scale photonic crystal resonators," Phys. Rev. B **73**, 235117 (2006).
19. J. Vŭcković, M. Lončar, H. Mabuchi, and A. Scherer, "Optimization of Q factor in microcavities based on freestanding membranes," IEEE J. Quantum Electron. **38**, 850-856 (2002).
20. S.-H. Kim, M.-K. Seo, J.-Y. Kim, and Y.-H. Lee, "Effects of a bottom substrate on emission properties of a photonic crystal nanolaser," IPRM 07, IEEE 19th International Conference on, 480-483 (2007).
21. D.-J. Shin, S.-H. Kim, J.-K. Hwang, H.-Y. Ryu, H.-G. Park, D.-S. Song, and Y.-H. Lee, "Far- and near-field investigations on the lasing modes in two dimensional photonic crystal slab lasers," IEEE J. Quantum Electron **38**, 857-866 (2002).
22. W. H. Press, S. A. Teukolsky, W. T. Vetterling, and B. P. Flannery, *Numeric Recipes in C: The Art of Scientific Computing, 2nd ed*. (Cambridge University Press, Cambridge, England, 1992), p.108.
23. A. Taflove and S. C. Hagness, *Computational Electrodynamics: The Finite-Difference Time-Domain method, 2nd ed.* (Artech House, Norwood, MA, 2000).
24. Y. Akahane, T. Asano, B.-S. Song, and S. Noda, "Fine-tuned high-Q photonic-crystal nanocavity," Opt. Express **13**, 1202-1214 (2005).
25. D. Englund, I. Fushman, and J. Vŭcković, "General Recipe for Designing Photonic Crystal Cavities," Opt. Express **12**, 5961-5975 (2005).
26. J.-K. Yang, M.-K. Seo, I.-K. Hwang, S.-B. Kim, and Y.-H. Lee, "Polarization-selective resonant photonic crystal photodetector," Appl. Phys. Lett. **93**, 211103 (2008).
27. S. Noda, A. Chutinan, and M. Imada, "Trapping and emission of photons by a single defect in a photonic bandgap structure," Nature **407**, 608-610 (2000).

1. Introduction

A single-cell photonic-crystal (PhC) cavity [1-4] with high quality (Q) factor and small mode volume can realize various high-performance photonic applications and quantum optical phenomena such as low-threshold lasers [5], cavity quantum electrodynamics (CQED) experiments [6], single photon sources [7] and high-speed modulation [3, 8]. This cavity can also be used for the sensitive biochemical detection by utilizing its high electromagnetic field localization [9-11]. In general, the photons coming out of such a wavelength-scale cavity are highly diverging due to the strong diffractive tendency [12], but the vertical emission and efficient collection of light are crucial for practical applications. While dipole-type modes exhibit vertical emission naturally [13, 14], both the relatively-low Q factor and degeneracy of the dipole mode limit its quantum optical applicability. Furthermore, for the electrical pumping, Q factor of the dipole mode decreases greatly because the electric field maximum at the center of dipole mode is strongly disturbed due to the central dielectric post which is underneath the PhC slab for current injection [15, 16]. Alternatively, the nondegenerate hexapole mode, one of the whispering-gallery-type modes, is more attractive thanks to the high Q factor of ~10^6 and the small mode volume [4, 17]. The hexapole mode has an electric field node at the center and thus can be used for the electrically-pumped PhC laser [16]. However, the typical hexapole mode has a null vertical emission and it is hard to funnel photons into a conventional optical system. Recently, it has been theoretically proposed that linearly-polarized vertical beaming from the hexapole mode can be obtained by simple modification of the single-cell PhC cavity, so that highly efficient coupling into a single mode fiber is achievable [18]. In this study, we experimentally demonstrate linearly-polarized efficient vertical emission from the hexapole mode of a modified single-cell PhC resonator.

#107732 - $15.00 USD Received 24 Feb 2009; revised 28 Mar 2009; accepted 28 Mar 2009; published 31 Mar 2009

2. Engineered hexapole mode for linearly-polarized vertical beaming

Figure 1(a) shows the schematics of a single-cell PhC cavity based on InGaAsP PhC slab and InP substrate. As suggested by Kim et al, hexapole mode photons could be engineered to go out vertically by destroying the balance of the electric field distribution [18]. We enlarge two nearest neighbor holes around the cavity along the *x*-direction as shown in Fig. 1(b). Then the vector summation of E_x fields that have even symmetry becomes non-zero and *x*-polarized photons are allowed to scatter out along the vertical direction. In comparison, the summation of E_y fields that have odd symmetry remain very close to zero, because each positive E_y component is always cancelled by a partner E_y component of an opposite sign (Fig. 1(c)). The net effect, therefore, shows up as highly *x*-polarized vertical emission. This loss engineering reduces the theoretical Q factor of hexapole mode to 20,000 [18], still larger than that of a conventional dipole mode [19]. Furthermore, we can achieve even smaller divergent angle of emission by choosing the air gap size (Fig. 1(a)) encouraging the constructive interference [20]. In this study, we measure the far-field emission patterns of the hexapole mode in this "engineered" single-cell PhC cavity of Fig. 1(b) and demonstrate directional and linearly-polarized emission properties.

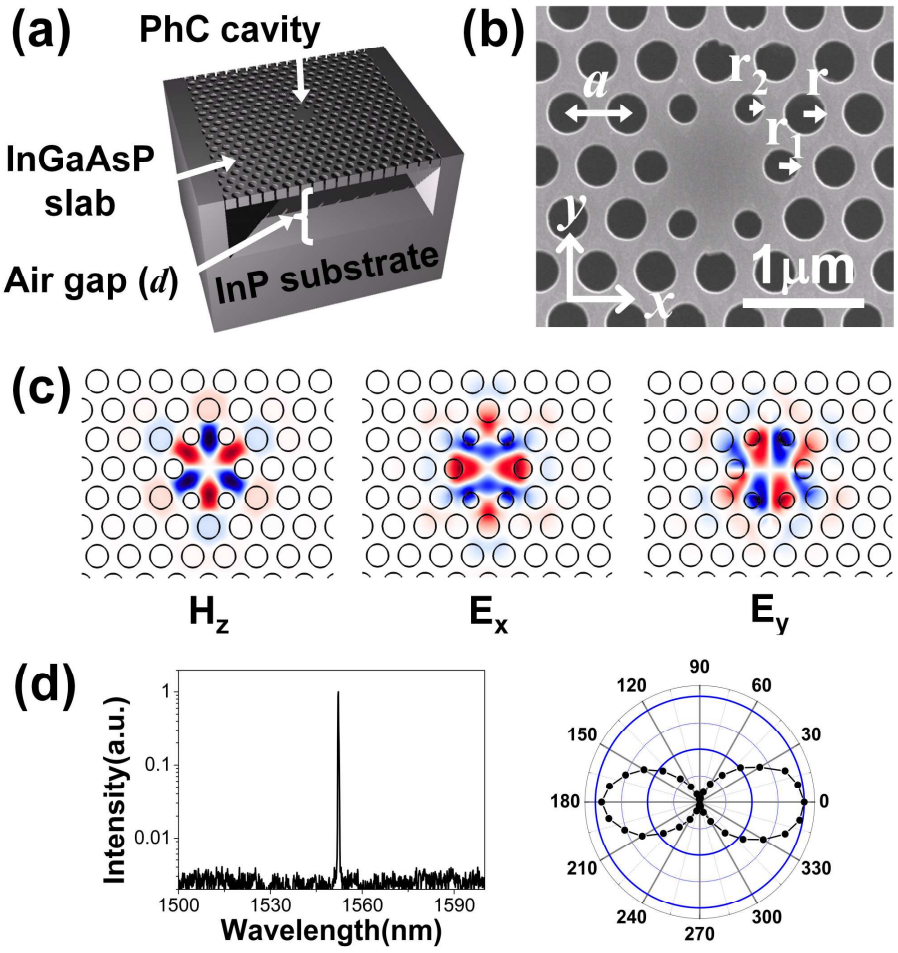

Fig. 1. (a) Schematics of a single-cell PhC cavity built on InGaAsP slab and InP substrate. (b) Scanning electron microscope image of an engineered single-cell PhC cavity. The radii of two nearest neighbor air holes on the *x*-axis (r_1) are increased up to 0.29*a*. (c) The calculated H_z, E_x and E_y field profiles of the engineered hexapole mode. (d) Measured lasing spectrum and polarization characteristics of the engineered hexapole mode.

#107732 - $15.00 USD Received 24 Feb 2009; revised 28 Mar 2009; accepted 28 Mar 2009; published 31 Mar 2009

The engineered single-cell PhC laser is fabricated using the procedures described in our previous reports [2]. Three pairs of InGaAsP quantum wells emitting near 1.5 μm are embedded in a 280 nm-thick free-standing slab and the air gap size *d* is 860 nm (Fig. 1(a)). The lattice constant (*a*) of the fabricated PhC structure is 500 nm. The radii of the regular air holes (r), two enlarged nearest neighbor air holes along the *x*-axis (r_1) and the other four nearest neighbor air holes around the cavity (r_2) are 0.35*a*, 0.29*a* and 0.25*a*, respectively (Fig. 1(b)). We perform a photoluminescence (PL) spectroscopy to measure the optical characteristics of this engineered single-cell PhC cavity. The cavity is pulse pumped by a 980-nm InGaAs laser diode (10 ns pulses of ~1% duty cycle). Using a 50x objective lens, we focus the pump beam to ~3.5 μm and collect light from the cavity. We observe single lasing peak of the hexapole mode (λ = 1552.2 nm) from the cavity of Fig. 1(b) as shown in the above-threshold PL spectrum (Fig. 1(d)). The emission of the engineered hexapole mode laser is strongly *x*-polarized and the polarization extinction ratio (PER) is measured to be 45:1. The numerical aperture of our objective lens is 0.5. The theoretical PER of 60:1 is slightly larger than the measured value.

3. Polarization-resolved far-field measurement

3.1. Solid scanning system for far-field measurement

We measure the far-field emission patterns of the lasing modes using the experimental setup of Fig. 2 [21]. In order to fully characterize the laser emission over the whole upper hemisphere, we rotate both of the sample and the photodetector. The photodetector scans from -90° to 90° in the polar (θ-) direction and from 0° to 180° in the azimuthal (ϕ-) direction, respectively. Because a size of detector cell and a distance between the sample and the detector are 1 mm^2 and 30 cm, the angular resolution limit of our measurements can be reduced to 0.2°. In these experiments, however, scanning steps of the angles in θ- and ϕ-directions are roughly set to 10° and 9°, respectively, to decrease total measuring time. The polynomial-interpolation is used to draw smooth far-field emission patterns [22]. To optically excite resonant modes, a 980-nm pumping laser beam is positioned on the backside of the transparent InP substrate. A polarizer is placed in front of the photodetector to measure polarization-resolved far-field emission patterns. The raw data obtained from the measurements over the curved surface of the upper hemisphere are projected onto a two dimensional (2-D) flat surface using a mapping defined by $x = \theta\cos\phi$ and $y = \theta\sin\phi$ to clearly understand the complicated three dimensional (3-D) emission patterns (the inset of Fig. 2).

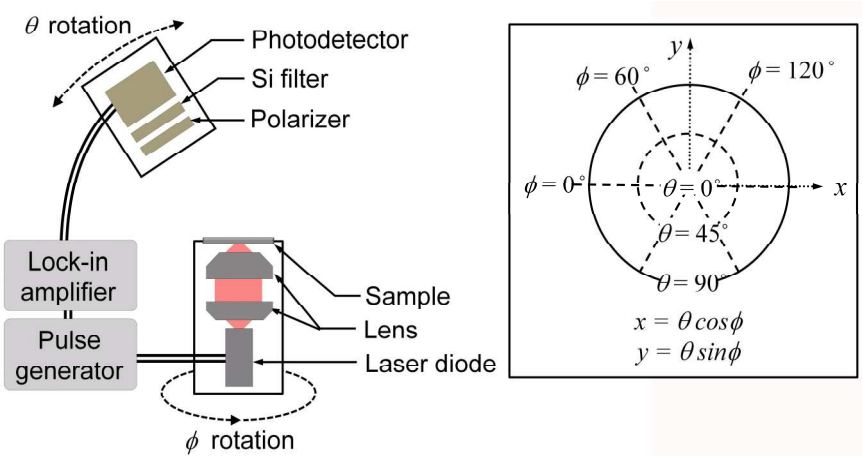

Fig. 2. Schematics of far-field measurement setup (left) and projection of the curved surface onto a 2-D flat surface (right).

#107732 - $15.00 USD Received 24 Feb 2009; revised 28 Mar 2009; accepted 28 Mar 2009; published 31 Mar 2009

3.2. Far-fields of the engineered hexapole mode laser

Figure 3(a) shows the measured far-field emission patterns of the hexapole mode in the engineered PhC cavity. Note that the vertical beaming is successfully demonstrated from the engineered PhC cavity as expected (Fig. 3(a)). Thus, a large fraction of light is emitted into the vertical direction: 56% of the photons are emitted within a divergence angle of ±30°. We also investigate the cross-sectional intensity distribution of this far-field emission pattern. As shown in Fig. 3(b), the measured cross sectional views along the *x*- and *y*-axes (black lines) agree well with the results (red dotted lines) obtained by 3-D finite-difference time-domain (FDTD) method. It is interesting that the Gaussian-like far-field emission pattern is obtained through the simple modification of the cavity. In the cross section along the *y*-axis, there are two additional weak lobes at an angle near $\theta = \pm 65°$. This will be discussed in Sec. **4**. In addition, we measure the polarization-resolved far-field emission patterns (Figs. 3(c) and 3(d)). θ- and ϕ-components of the hexapole mode each have two intensity lobes, for which these pairs of lobes are perpendicular to each other and have singularities at the central point (θ = 0°). This implies that the emission is linearly-polarized along the *x*-direction. Consequently, the measured intensity distribution and polarization property strongly support that the engineered hexapole mode has the linearly-polarized Gaussian-like far-field emission pattern and thus can be well overlapped with the fundamental mode (LP01) of an optical fiber. We expect that the efficient light coupling of the PhC cavity to the fiber can be successfully achieved.

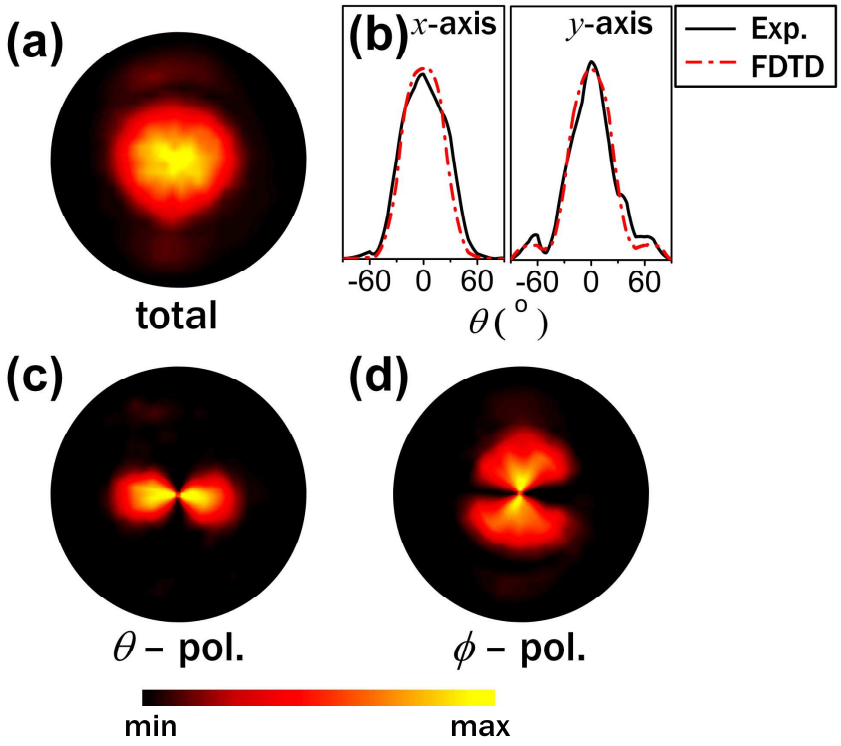

Fig. 3. (a) Measured far-field emission patterns in the engineered hexapole mode. (b) Cross sectional scan of the total intensity along *x*- (left) and *y*-axes (right). The measurements (black lines) agree well with the 3-D FDTD simulation results (red dotted lines). (c)-(d) Measured polarization-resolved far-field emission patterns. θ- and ϕ-polarization components are measured in (c) and (d), respectively.

#107732 - $15.00 USD Received 24 Feb 2009; revised 28 Mar 2009; accepted 28 Mar 2009; published 31 Mar 2009

3.3. Far-fields of the reference hexapole mode laser

We compare the far-field emission patterns of the engineered hexapole mode with those of the reference to confirm the effect of the modification. Figure 4 shows the far-field emission patterns of the reference hexapole mode without modification. As shown in Fig. 4(b), the structural parameters of the reference PhC cavity are identical to those of the engineered cavity of Fig. 1(a) except the radii of two nearest neighbor air holes on the *x*-axis. Observe that the far-field of the reference hexapole mode presents no emission along the vertical direction. Only 15% of the photons of the reference hexapole mode are contained within a divergence angle of ±30°. This value compares reasonably with that (13%) of 3-D FDTD method. Although 3-D FDTD method predicts six lobes in the far-field of the reference hexapole mode (Fig. 6(a)), those lobes are not clearly observable in the real measurement (Fig. 4(a)). In fact, the small structural imperfections accumulated during the fabrication process show up as an unbalance in the far-field emission pattern as shown in Fig. 4(a). In the polarization-resolved measurements, θ- and ϕ-components show recognizable six lobes and the direction of those lobes of θ-component is rotated by 30° relative to those of ϕ-component. This typical property of a whispering gallery-like mode shows that the reference hexapole mode has no preferred polarization direction and agrees well with the simulation results (Figs. 6(b) and 6(c)). We expect that these polarization-resolved far-field measurements can be useful for identifying the resonant modes of a single-cell PhC cavity.

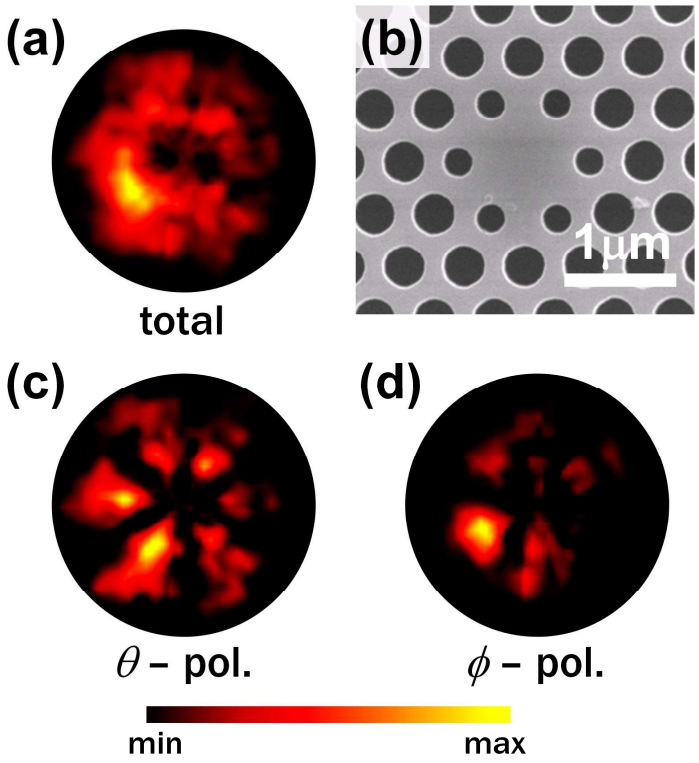

Fig. 4. (a) Measured far-field emission pattern in the reference hexapole mode. (b) SEM image of a reference single-cell PhC cavity. (c)-(d) The polarization-resolved far-field emission patterns. θ- and ϕ-polarization components are measured in (c) and (d), respectively.

#107732 - $15.00 USD Received 24 Feb 2009; revised 28 Mar 2009; accepted 28 Mar 2009; published 31 Mar 2009

4. 3-D FDTD simulations of polarization-resolved far-field emission patterns

To better understand the experimental results, 3-D FDTD simulations are performed to analyze the characteristics of the far-field emission patterns in both engineered and reference hexapole modes (Figs. 5 and 6). We compute the far-field emission patterns transformed from the near-field distribution using fast Fourier transform (FFT) algorithm [18, 23]. This method has been also used for Q-factor optimization [12, 19, 24, 25]. As shown in Fig. 5, one can easily see that Gaussian-like vertical beaming profile and linear polarization agree with those of the fabricated sample (Fig. 3). Although the structural perturbations degrade the quality factor noticeably, vertical beaming characteristics did not change as sensitively. However, when the relative air-hole size deviates more than ±5%, the output tends to diverge significantly [20]. The fraction of photons emitted within ±30° of the engineered hexapole mode is calculated as 67%. In comparison, that of dipole-type mode is reported as 30% [13]. The calculated θ- and ϕ-polarization resolved far-field patterns (Figs. 5(b) and 5(c)) agree well with measured data (Figs. 3(c) and 3(d)). One can also confirm in Figs. 5(d) and 5(e) that the vertical output is strongly x-polarized.

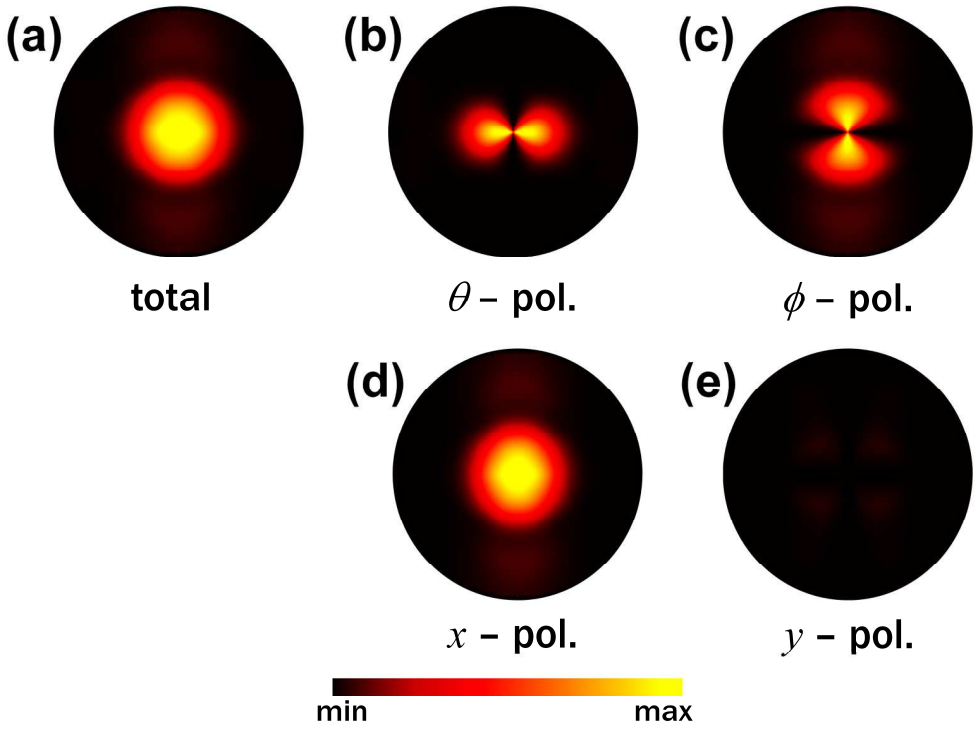

Fig. 5. 3-D FDTD simulation results of the far-field emission patterns in the engineered hexapole mode. (a) Total intensity, (b) θ-, (c) ϕ-, (d) x- and (e) y-polarization components of far field patterns are computed.

#107732 - $15.00 USD Received 24 Feb 2009; revised 28 Mar 2009; accepted 28 Mar 2009; published 31 Mar 2009

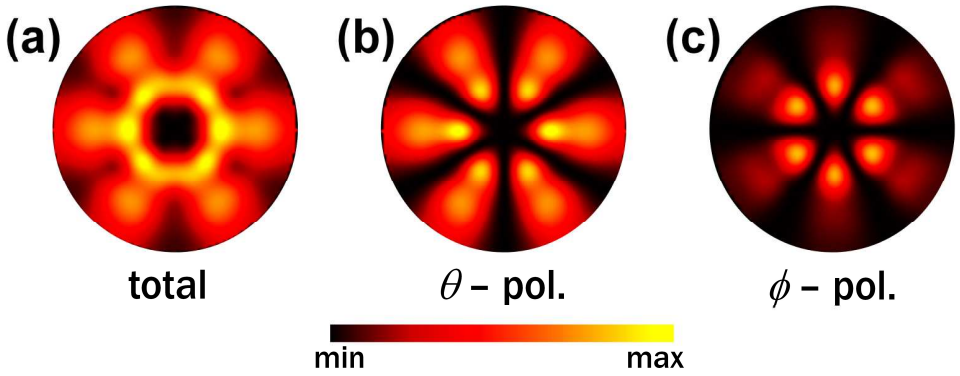

Fig. 6. 3-D FDTD simulation results of the far-field emission patterns in the reference hexapole mode. (a) Total intensity, (b) θ-, and (c) ϕ-polarization components of far-field patterns are computed.

In these simulations, we apply the InP bottom substrate under the PhC slab as shown in Fig. 1(a). Since the reflectance between the air and the simple InP bottom substrate is around 30%, the reflection from the bottom substrate can increase the vertical out-coupling of total radiated power [20]. In our fabricated structure, the ratio of the vertical emitting power to total power is calculated 64%. In addition, the far-field emission pattern can be optimized by controlling the distance between the PhC slab and the bottom substrate and reflectance of the bottom substrate [18, 20]. Near the constructive interference condition for vertical reflection, $2d = 1\lambda, 2\lambda, 3\lambda \ldots$, vertical beaming is achievable. We choose air gap size near 0.5λ because smaller air gap size is preferred for making current flowing dielectric post [15, 16]. We can also see that the additional two weak lobes are along the y-axis at $\theta = 65°$ in Fig. 5. Because the air gap distance d between the PhC slab and the bottom substrate is 860 nm, destructive interference makes the intensity node at $\theta = 42°$, which can be obtained by the formula, $2d/\cos\theta = 1.5\lambda$. This value agrees well with the experimental result (Fig. 3).
We expect that, based on the effect of vertical coupling, this engineered hexapole mode can be employed for micro-photodetector [26] and vertical add-drop devices for photonic integrated circuits [27].

5. Summary

We successfully demonstrate vertical funneling from the engineered hexapole mode of a single-cell PhC cavity using the far-field measurement system. 56% of linearly-polarized light of the resonant mode are measured within a divergence angle of ±30°. With this vertical beaming scheme, the efficient coupling of light from a wavelength-scale cavity with a fundamental mode (LP01) of an optical fiber is expected.

Acknowledgments

This work was supported by the Korea Science and Engineering Foundation (KOSEF) (No.ROA-2006-000-10236-0), the Korea Foundation for International Cooperation of Science and Technology (KICOS) (No. M60605000007-06A0500-00710) through grants provided by the Korean Ministry of Science and Technology (MOST) and the Star-Faculty Project (Grant No. KRF-2007-C00018). H.G. P. acknowledges support by the Korea Research Foundation Grant funed by the Korean Government (KRF-2008-331-C00118) and the Seoul R&BD Program.

#107732 - $15.00 USD Received 24 Feb 2009; revised 28 Mar 2009; accepted 28 Mar 2009; published 31 Mar 2009